Learning Scale-Adaptive Tight Correlation Filter for Object Tracking

Shunli Zhang, Wei Lu, Weiwei Xing, and Li Zhang

***Abstract*—In this paper, we propose a novel tracking method by formulating tracking as a correlation filtering as well as a ridge regression problem. First, we develop a tight correlation filter-based tracking framework from the signal detection perspective. In this formulation, the correlation filter is set as the same size as the target, which can make full use of the relations of the adjacent image patches and effectively exclude the influence of the background. Specifically, we point out that the novel correlation filter model can be regarded as the ridge regression model which takes into account the different importance of the samples and has the consistent objective with tracking. Second, we focus on the scale variation problem in tracking. By making use of the spatial structure of the correlation filter, the multiscale filter banks can be generated via interpolation to handle the scale estimation problem easily. Third, we present a novel distance importance-based confidence calculation model to determine the final tracking result, which not only makes use of the fine discriminability of the correlation filter but also takes the distance importance of the candidate samples into account to alleviate the impact of similar distractors. Experimental results demonstrate that our method is superior to several state-of-the-art trackers and many other correlation filter-based methods in the benchmark datasets.**

***Index Terms*—Correlation filter, object tracking, ridge regression, scale adaption.**

I. Introduction

OBJECT tracking is a hot topic in computer vision. Due to its wide applications in motion analysis, video surveillance, human–computer interface, etc., it has attracted much attention recently. However, because of various complex factors, for example, occlusion, deformation, illumination variation, scale variation, fast motion, and background clutter, tracking is still a challenging task [1]–[3].

A typical tracking system often has three modules, that is, the appearance model, the motion model, and the update model. The appearance model, which plays a crucial role, can be divided into two types. The first is the generative model [4]–[9], which only uses the information of the target. The second is the discriminative model [10]–[13], which often formulates tracking as a binary classification problem and is known as the tracking-by-detection method. Since the latter model adopts the information of both the background and the target, it seems to offer more accurate and robust representation.

However, there are still some potential issues in existing tracking-by-detection methods. First, it is pointed out that the objectives of the tracker and the classifier are not consistent in many methods, where the objective of the tracker is to find the optimal location of the target precisely while the objective of the classifier is to predict the labels of the samples accurately [14]. Second, the training samples are often undersampled randomly and assigned to equal weights. This sampling strategy does not make full use of the spatial constraints around the target and ignores the different importance of the samples [15]. Besides the above issues, we also find that the high spatial correlations of adjacent image patches do not get enough attention, which increases the complexity of sampling, training, and detection. Furthermore, the size of the tracker is often fixed and the inner structure of the tracker is often neglected, so that the scale variation is not well addressed. These issues may be important factors affecting the tracking performance. Although some of these issues have been pointed out by some researchers, they have not been taken into account in a unified framework.

Recently, many correlation filter-based tracking methods have been proposed and achieved great success. These methods formulate tracking as a ridge regression problem, which can make full use of the spatial information and solve the downsampling issue in the binary classification model. Besides, the correlation filter-based methods transfer the ridge regression to a correlation filter problem by the circulant structure assumption, which can be realized by fast Fourier transformation (FFT) with high efficiency. Although these methods obtain both high tracking accuracy and fast tracking speed, there still exist some issues which degrade the performance of the trackers. For example, the correlation filter in [15]–[18] is obtained based on the circulant structure assumption, where the samples are represented by rectangle boxes larger than the true target and are implicitly generated by cyclic shift of the original target. As Fig. 1(a) shows, the samples with

Manuscript received May 6, 2018; revised July 26, 2018; accepted August 29, 2018. Date of publication September 26, 2018; date of current version October 22, 2019. This work was supported in part by the National Natural Science Foundation of China under Grant 61601021, Grant U1533132, and Grant 61370128, in part by the Beijing Natural Science Foundation under Grant L172022, in part by the Program for New Century Excellent Talents in University under Grant NCET-13-0659, in part by the China Postdoctoral Science Foundation under Grant 2017M610758, and in part by the Fundamental Research Funds for the Central Universities under Grant 2016RC015. This paper was recommended by Associate Editor Y. Yuan. *(Corresponding author: Shunli Zhang.)*

S. Zhang, W. Lu, and W. Xing are with the School of Software Engineering, Beijing Jiaotong University, Beijing 100044, China (e-mail: slzhang@bjtu.edu.cn; luwei@bjtu.edu.cn; wwxing@bjtu.edu.cn).

L. Zhang is with the Department of Electronic Engineering, Tsinghua University, Beijing 100084, China (e-mail: chinazhangli@tsinghua.edu.cn).

Color versions of one or more of the figures in this paper are available online at http://ieeexplore.ieee.org.

Digital Object Identifier 10.1109/TCYB.2018.2868782

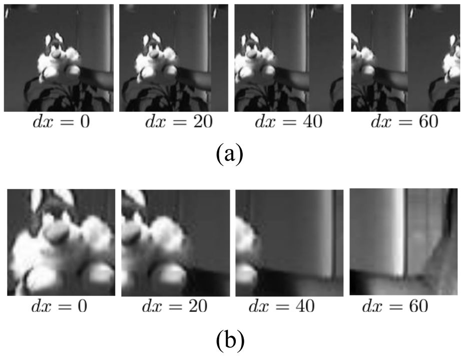

Fig. 1. Issue of the generated training samples for learning the correlation filters in methods [15]–[18]. Note that the samples in (a) are virtual while the samples in (b) are real.

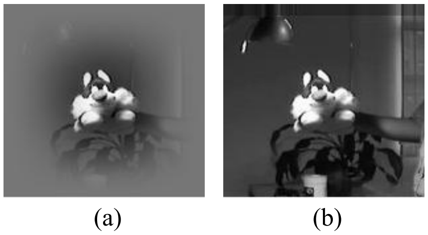

Fig. 2. Issue of the training patch in traditional correlation filter-based methods. Note that the training patch changes the information far away from the center in the traditional correlation filter (a), while it retains the original information of the image in our formulation (b).

horizontal translation $dx = 20$, $dx = 40$, and $dx = 60$ pixels are obtained by cyclic shift of the original sample with $dx = 0$. However, it should be noted that these samples do not fit the real scene, as the sample with $dx = 60$ pixels displays. In addition, in order to make the samples satisfy the circulant structure assumption, a bounding box used to represent the sample should be much larger than the target and a Hanning window must be utilized to deal with the discontinuity of the image margin, which leads to two additional problems. As Fig. 1(a) displays, the large bounding box contains much more background information which may not represent the target appearance accurately and brings more challenges to scale adaption and robustness to background changes. Besides, the Hanning window also changes the appearance of the training patch, adding the representation errors, as Fig. 2 illustrates.

In this paper, we propose a novel tracking method by learning a scale-adaptive tight correlation filter, attempting to address the above issues in tradition tracking-by-detection methods and in conventional correlation filter-based methods. First, we formulate tracking as a correlation filtering problem from the signal detection perspective and learn a tight correlation filter as the tracker, which does not need the prior assumption existing in other correlation filter-based methods. By taking the target as the signal of interest to detect, the objective of filtering is to find the optimal response corresponding to the target, which is consistent with the objective of tracking. Since the filter is set as the same size as the target, it is tight and can effectively reduce the effect of the background, as Fig. 1(b) shows. The samples corresponding to the correlation filter are real rather than virtual, which improves the representation accuracy. In addition, we establish the relationship between the proposed correlation filtering formulation and the ridge regression model from the practical physics background, which enriches the tracking-by-detection framework. Different from the binary classification formulation which assigns discrete labels to samples, in our method, we would like to build a ridge regression model to assign continuous values to samples. Specifically, we point out that the correlation filter is a specific realization of the ridge regression, and the correlation filter corresponds to the appearance model of the tracking-by-detection framework.

Second, we present a multiscale strategy to handle the scale estimation problem adaptively by using the spatial structure of the correlation filter. In our method, the learned correlation filter has the same size with the target. Since the filter retains the spatial structure in the 2-D plane, the multiscale filter banks can be approximately implemented based on the interpolation technique, which can be used for multiscale filtering. Then, the target scale can be estimated adaptively by exploring the optimal response on multiple scales heuristically. The experimental results in the benchmark datasets demonstrate that our method can achieve desirable tracking performance and outperform many state-of-the-art trackers, especially in the condition of scale variation.

Third, we develop a novel location method in the motion model by making use of both the correlation filter and the distance importance weight of the candidate samples. In most traditional tracking-by-detection and correlation filter-based methods, the confidence score is obtained by only the appearance model, for example, the classifier or the correlation filter, and the candidate samples are assigned to the same importance. However, in this condition, the similar distractor, which is far away from the target, may cause the tracking drift. In this paper, we consider the impact of the distance corresponding to each candidate sample as well as the confidence obtained by the correlation filter. In other words, the final confidence map is the combination of the distance importance score and the filtering result, which can effectively reduce the impact of the similar distractors.

The main contributions of this paper are three-fold.

1) We formulate tracking as a tight correlation filtering problem instead of the circulant structural assumption-based correlation filtering. In this formulation, the size of the correlation filter is set the same as the target, which can effectively avoid the effect of the virtual samples and reduce the influence of the background information. Specifically, the zero padding and cropping strategy are introduced to efficiently realize the learning of the filter and tracking in the Fourier domain, which does not need the circulant assumption and can effectively address the boundary effect issue.
2) We approximately construct the multiscale filter banks for scale adaption based on the interpolation strategy and dense feature extraction. Since the multiscale filters are directly built in the filter domain, our method may locate the target more precisely than many other scale

adaptive methods which realize scale adaption by scaling the images.

3) We present a novel location strategy to determine the tracking result which considers both the filtering result and the distance importance of the candidate samples. On one hand, the filtering results obtained by the multiscale filter banks reflect the basic location information from the appearance model. On the other hand, the distance importance of the candidate samples is taken into account, which can effectively alleviate the impact of the similar distractors.

The remainder of this paper is organized as follows. In Section II, we review the tracking-by-detection methods, and talk about the correlation filter-based tracking methods. Section III formulates tracking as a correlation filtering problem and explains it from the perspective of ridge regression. The detailed realization of the proposed method is shown in Section IV and the experimental results are displayed in Section V. Section VI concludes this paper.

II. Related Work

A. Tracking-by-Detection

Tracking-by-detection methods often formulate tracking as a binary classification problem [10], [19]–[24]. Thus, different classifiers, for example, support vector machine and boosting, have been applied to build the trackers. However, there are some potential issues in most of the above methods, for example, the neglect of the different importance of the samples, the inconsistency of the objectives, and the undersampling strategy, which may degrade tracking performance. To address the above issues, Babenko *et al.* [11] introduced the online multiple-instance learning into tracking. They replace the positive and negative samples by the positive and negative bags to train the classifier, alleviating the drift caused by the classification inaccuracies and sample ambiguity to some degree. Hare *et al.* [14] applied the structured output learning in tracking to address the inconsistency of the objectives of tracking and classification. In their method, the importance of the samples is measured implicitly. Possegger *et al.* [25] presented a discriminative object model capable of differentiating the object of interest from the background. This method relies on standard color histograms and is used to identify and suppress distracting regions in advance. Different from the above formulations, in this paper, the correlation filter can be considered as a novel ridge regression model, which can measure the importance of the samples explicitly and adopt a dense sampling strategy to make use of the spatial constraints. Besides, the objectives of the regression and tracking are consistent, providing a model with finer discriminability.

Some other strategies which aim to build accurate appearance models have also been introduced to improve tracking performance. Wang *et al.* [26] proposed the multicue-based tracking method, which incorporates optical flow, color, and depth clues simultaneously. However, this method is based on the assumption that different features can provide complementary supporting information, which still belongs to the generative model. Fang *et al.* [27] presented the part-based online tracking method with geometry constraints and attention selection, which utilizes a part-based structure to construct an adaptive appearance model together with the attentional sample weighting and a two-stage motion model. Fang *et al.* [28] proposed an online hashing tracking method by exploiting the spatiotemporal saliency for template sampling. By making use of the hash code learning, the useful relationship between the positive and negative templates can be preserved and matching can be efficiently conducted. The latter two methods can be considered as the discriminative models, which utilize the positive and negative samples-based classification models. In our method, although we mainly adopt the histogram of the oriented gradients (HOGS) feature for representation, the correlation filtering formulation can better use spatial information by dense sampling, which can build a more accurate discriminative appearance model.

B. Correlation Filter-Based Tracking

The correlation filter has achieved success in many domains [16], [29], [30]. Recently, some tracking methods based on the correlation filter have been proposed. Bolme *et al.* [31] proposed a minimum output sum of a squared error filter for tracking, which first models the appearance adaptively by learning the correlation filter but does not make full use of the spatial constraints. Henriques *et al.* [15] developed the circulant structure of tracking-by-detection with kernels tracker (CSK) by exploiting the circulant structure of the local image patch and learning a kernelized least squares classifier. Note that the size of the learned filter is much larger than the target due to the circulant structure assumption. They further propose the kernelized correlation filter tracker (KCF) [16] by utilizing the HOG feature instead of the intensity, which significantly improves CSK. Danelljan *et al.* [32] developed the adaptive color attributes tracker (CN) by adding the color attribute to augment the feature used by CSK. Recently, some researchers [33]–[36] propose new tracking methods by combining both the deep convolutional neural networks and correlation filter, which can further improve tracking performance. However, most of these methods are based on the circulant structure assumption, and use a rectangle with much larger size to represent the object, that is, the filters are not tight. Although we also employ the concept of correlation filter, we stress that our formulation is different from the above methods. We argue that the circulant structure assumption in those methods is not often satisfied, especially in the condition of complex backgrounds. Moreover, when the target moves, the changes of its surrounding background may be larger than itself, making the assumption invalid. In our method, we model tracking from the signal detection viewpoint, which does not need the above assumption. We build a new correlation filter framework by setting the filter as the same size as the target, which is tight and can exclude the effect of the background as far as possible.

Some researchers also extend the KCF method to the scale-adaptive versions by introducing the multiscale strategy. Danelljan *et al.* [17] presented discriminative scale space tracking (DSST) and attempt to address the scale variation under the correlation filter framework by learning separate filters for translation and scale estimation, respectively, but the scale estimation depends on the accuracy of the position. Li and Zhu [18] proposed scale adaptive with a multiple features tracking approach (SAMF) which takes the color-naming feature to improve the representation and employs bilinear interpolation to generate image representations in multiple scales. Both of these two methods realize the scale adaption by interpolation in the image domain and extract features many times. Further, Zhang *et al.* [37] presented the fast tracking via spatiotemporal context learning (STC), which employs a similar framework to CSK and is explained from the spatial–temporal context perspective. Besides, they add a scale-adaption mechanism to handle the scale estimation in closed form. Huang *et al.* [38] developed a novel strategy to deal with the scale changes, which integrates the class-agnostic detection proposal method into a correlation filter tracker and uses the EdgeBoxes to realize the scale and aspect ratio adaption. Different from the above methods, the proposed scale adaption in our method directly works in the filter domain, which makes use of the inner structure of the filter. Besides, because the image region is not scaled, our method may provide a more precise location.

III. Formulation

A. Correlation Filtering Formulation

Different from most of the traditional correlation filter-based tracking methods which are obtained from the regression formation in the mathematical domain, we formulate tracking as a correlation filtering problem from the perspective of signal detection which has a practical physics background. By taking the image patch as an input signal and the tracker as a filter, tracking can be modeled as a correlation filtering process to detect the signal of interest, where the largest response value corresponds to the target. To make the objectives of tracking and filtering consistent, it is necessary to design a specific response function, whose value is largest in the target position and becomes smaller with the increasing distance to the target. In practice, the correlation filter can be learned based on the known image patch and its response, and applied for filtering in the testing image.

As Fig. 3 illustrates, the proposed tracking framework based on correlation filtering includes two components, that is, learning the filter and tracking by filtering. In the learning stage [Fig. 3(a)], denote the training region as $\mathbf{f}$ which centers at the target, and the response function is $\mathbf{g}$. Hereby, the Gaussian function is regarded as the response function. The correlation filter $\mathbf{h}$ is learned according to $\mathbf{f}$ and $\mathbf{g}$. Note that the $\mathbf{h}$ is tight and its size is $v \times w$, which is the same as the target, and the size of $\mathbf{f}$ is $V \times W$. Based on the minimum output squared error criterion, the objective function of learning the required correlation filter is

$$\min_{\mathbf{h}} \|\mathbf{f} \otimes \mathbf{h} - \mathbf{g}\|^2 + \lambda\|\mathbf{h}\|^2 \tag{1}$$

where $\otimes$ denotes the correlation operation, and λ is the tradeoff parameter.

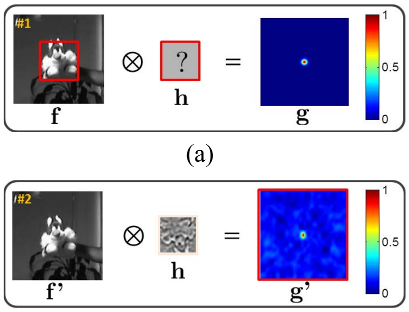

(a)

(b)

Fig. 3. Formulating tracking as a correlating filtering problem. (a) In the learning stage, the correlation filter $\mathbf{h}$ is learned based on the training patch $\mathbf{f}$ and the predefined response $\mathbf{g}$. (b) In the tracking stage, the response $\mathbf{g}'$ is obtained by applying the filter $\mathbf{h}$ in the testing patch $\mathbf{f}'$ to determine the optimal tracking result.

However, the correlation operation in (1) makes it hard to optimize the objective function directly. Therefore, we introduce the zero padding strategy to turn the linear convolution into the circulant convolution. According to the Parsevals identity [39], the circulant convolution can be realized by FFT efficiently. After padding zeros in $\mathbf{h}$ and $\mathbf{f}$, we can get the augmented $\bar{\mathbf{h}}$ and $\bar{\mathbf{f}}$. Then, (1) can be rewritten in the Fourier domain

$$\min_{\hat{\mathbf{h}}} \|\hat{\mathbf{f}} \odot \hat{\mathbf{h}}^* - \hat{\mathbf{g}}\|^2 + \lambda\|\hat{\mathbf{h}}^*\|^2 \tag{2}$$

where $\hat{\mathbf{h}} = \mathcal{F}(\bar{\mathbf{h}})$, $\hat{\mathbf{f}} = \mathcal{F}(\bar{\mathbf{f}})$, $\hat{\mathbf{g}} = \mathcal{F}(\mathbf{g})$, $*$ denotes the complex conjugation, $\mathcal{F}$ denotes the FFT, and $\odot$ denotes the element-wise product. The zero padding strategy makes FFT feasible and does not depend on the circulant structure assumption in previous methods. Then, the objective function in (2) can be optimized by

$$\hat{\mathbf{h}} = \frac{\hat{\mathbf{f}} \odot \hat{\mathbf{g}}^*}{\hat{\mathbf{f}} \odot \hat{\mathbf{f}}^* + \lambda}. \tag{3}$$

Correspondingly, the augmented correlation filter in the spatial domain can be obtained by $\bar{\mathbf{h}} = \mathcal{F}^{-1}(\hat{\mathbf{h}})$, where $\mathcal{F}^{-1}$ denotes the inverse FFT (IFFT). Then, $\mathbf{h}$ is cropped from $\bar{\mathbf{h}}$ to obtain the valid part with the same size as the target.

In the tracking stage [Fig. 3(b)], denote the candidate region of the next frame as $\mathbf{f}'$. Based on $\mathbf{h}$, the tracking is able to be conducted in $\mathbf{f}'$ by filtering in the spatial domain

$$\mathbf{g}' = \mathbf{f}' \otimes \mathbf{h}. \tag{4}$$

Further, the filtering can be efficiently conducted in the frequency domain by FFT and IFFT based on the augmented image patch $\bar{\mathbf{f}}'$ and the transformed $\hat{\mathbf{h}}$ after padding zeros

$$\mathbf{g}' = \mathcal{F}^{-1}(\mathcal{F}(\bar{\mathbf{f}}') \odot \hat{\mathbf{h}}^*) \tag{5}$$

where $\mathbf{g}'$ represents the obtained filtering results, the maximum of which corresponds to the optimal target position.

B. Ridge Regression Explanation

We formulate tracking as a ridge regression problem from the tracking-by-detection perspective and establish the relationship between the novel ridge regression formulation and

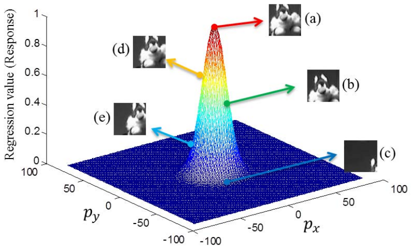

Fig. 4. Ridge regression framework for tracking. In this model, the samples are assigned to different Gaussian function values according to their distances to the target. As (a)–(e) show, the closer the sample is to the target, the higher regression value is assigned.

the above correlation filtering model. Different from the binary classification using the random undersampling manner, hereby, we utilize a dense sampling strategy. Assume that the position of the target in a frame is $\mathbf{p}(\mathbf{x}_0) = (p_{x0}, p_{y0})$, the position of the ith sample is $\mathbf{p}(\mathbf{x}_i) = (p_{xi}, p_{yi})$, the size of the target is $v \times w$, and the size of the sampling region is $V \times W$. The training samples will be cropped by sliding the sampling window around the target, following $\|p_{xi} - p_{x0}\| < ([W - w]/2)$ and $\|p_{yi} - p_{y0}\| < ([V - v]/2)$.

As Fig. 4 shows, the importance of the samples is different because they have different distances to the target. It is natural to assign a higher value to the sample which is closer to the target. Taking the Gaussian function as the predefined regression function, we can build the regression model by assigning continuous values to the samples according to their distances to the target. Assume that the discriminant function of the ridge regression is $f(\mathbf{x}) = \mathbf{w}^T\mathbf{x}$, which can be obtained by optimizing the following objective function:

$$\min_{\mathbf{w}} \sum_i \|\mathbf{w}^T\mathbf{x}_i - \mathbf{y}_i\|^2 + \lambda\|\mathbf{w}\|^2. \tag{6}$$

It is well-known that the above problem has a closed-form solution, which can be easily obtained by

$$\mathbf{w} = (\mathbf{X}^T\mathbf{X} + \lambda\mathbf{I})^{-1}\mathbf{X}^T\mathbf{y} \tag{7}$$

where $\mathbf{X} = (\mathbf{x}_1, \mathbf{x}_2, \ldots, \mathbf{x}_M)^T$, each row of which represents a sample $\mathbf{x}_i$, $\mathbf{y} = (\mathbf{y}_1, \mathbf{y}_2, \ldots, \mathbf{y}_M)^T$ represents the function values of $\mathbf{X}$, and $\mathbf{I}$ denotes the identity matrix. Once $\mathbf{w}$ is obtained, it can be used to calculate the regression values of the candidate samples in the next stage.

We stress that the ridge regression and the correlation filtering have a close relationship. For the function value of the sample $\mathbf{x}_i$ in position $\mathbf{p}(\mathbf{x}_i)$

$$\mathbf{y}_i = \mathbf{w}^T\mathbf{x}_i = \sum_j w_j x_{ij} \tag{8}$$

where w_j and x_{ij} are the jth elements of $\mathbf{w}$ and $\mathbf{x}_i$, respectively. The response value of the filter at this position is

$$\mathbf{g}_i = \sum_{j=1}^{w}\sum_{k=1}^{v} H(j,k)F_i(j,k) \tag{9}$$

where $H(j,k)$ and $F_i(j,k)$ represent the elements of $\mathbf{h}$ and the ith sample patch $\mathbf{f}_i$ cropped from $\mathbf{f}$, respectively. Note that $\mathbf{w}$ and $\mathbf{x}_i$ work in vector form, and $\mathbf{h}$ and $\mathbf{f}_i$ are in 2-D plane form. Under the condition of single-channel features, for example, intensity, it has $\mathbf{x}_i = \text{vec}(\mathbf{f}_i)$, where vec denotes the vectorizing operation. By (8) and (9), if we set $\mathbf{w} = \text{vec}(\mathbf{h})$, it can be observed that $\mathbf{y}_i = \mathbf{g}_i$. Therefore, the correlation filtering is a specific realization of the ridge regression model and accords with the tracking-by-detection framework. The relationship of these two formulations is also retained when multichannel features are used.

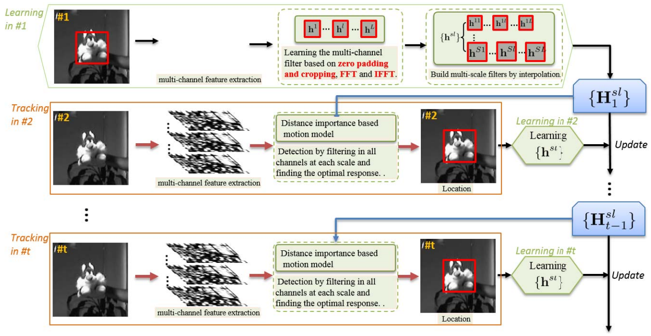
Learning in #1
#1
multi-channel feature extraction
$\mathbf{h}^1$ ... $\mathbf{h}^l$ ... $\mathbf{h}^L$
Learning the multi-channel filter based on zero padding and cropping, FFT and IFFT.
$\{\mathbf{h}^{sl}\}$
$\mathbf{h}^{11}$ ... $\mathbf{h}^{1l}$ ... $\mathbf{h}^{1L}$
$\mathbf{h}^{S1}$ ... $\mathbf{h}^{Sl}$ ... $\mathbf{h}^{SL}$
Build multi-scale filters by interpolation.
$\{\mathbf{H}_1^{sl}\}$
Tracking in #2
#2
multi-channel feature extraction
Distance importance based motion model
Detection by filtering in all channels at each scale and finding the optimal response. .
#2
Location
Learning in #2
Learning $\{\mathbf{h}^{sl}\}$
Update
$\{\mathbf{H}_{t-1}^{sl}\}$
Tracking in #t
#t
multi-channel feature extraction
Distance importance based motion model
Detection by filtering in all channels at each scale and finding the optimal response. .
#t
Location
Learning in #t
Learning $\{\mathbf{h}^{sl}\}$
Update

Fig. 5. Complete tracking framework of the proposed method. Note that it contains several detailed components, including the zero padding strategy, the multichannel filter construction, multiscale realization, update model, etc., for concrete realization.

Specifically, two benefits can be acquired from the correlation filtering formulation. On one hand, correlation filtering can greatly decrease computational complexity. The complexity of sampling and matrix inversion in ridge regression is $\mathcal{O}((V-v)(W-w)vw)$ and $\mathcal{O}(D^3)$, respectively, where D is the dimension size of the feature of a sample. However, for the filtering formulation, the complexity of FFT and IFFT is both $\mathcal{O}(L_vL_w\log(L_vL_w))$. In practice, because the relations of the adjacent image patches are not fully exploited in regression, there exist many redundant operations in sample selection and feature extraction. On the other hand, the correlation filter works in the 2-D plane with a spatial structure. Thus, it can be used to deal with the scale variation problem by scaling itself adaptively.

IV. Realization

Based on the above correlation filtering formulation, hereby, we introduce how to complete the tracking process in detail. The complete tracking framework is shown in Fig. 5. First, we learn the practical correlation filter by introducing several techniques. Specifically, we introduce the zero padding and cropping strategy to make the fast realization by FFT available, multichannel features are extracted to improve the discriminability, and the multiscale filter banks are built based on the interpolation strategy to realize scale adaption. Next, the learned multichannel multiscale filters are used to track the target in the next frame, where the optimal position and scale are determined by the distance importance-based model. Further, based on the tracking result in the current frame, a new group of filters is built and used to update the system filter banks. At last, the filtering and update steps are iterated to complete the tracking.

A. Learning the Correlation Filter

1) Implementation With Zero Padding and Cropping: As we have mentioned in Section III-A, the first step is to

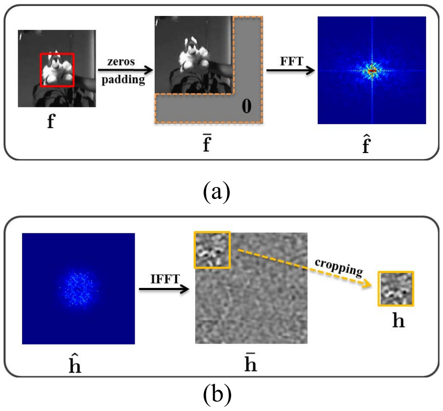

(a)

(b)

Fig. 6. Fast realization details of the tight correlation filter. On one hand, the zero padding strategy is used to ensure the consistence of the linear convolution and circulant convolution. On the other hand, cropping is utilized to generate the filter in spatial domain. (a) Fast correlation based on zero padding and FFT. (b) Calculating the filter in spatial domain with IFFT and cropping.

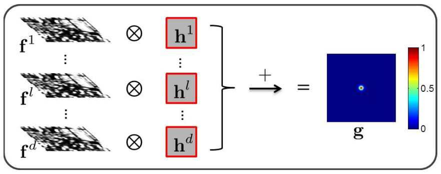

Fig. 7. Realization of the multichannel filter based on multichannel features.

construct the tight correlation filter. We employ a zero padding strategy to turn the correlation into circulant convolution which can be efficiently solved.

The reasons why the zero padding and cropping strategy are adopted to solve the optimization problem in (1) are as follows. First, the zero padding and cropping strategy is consistent with the tight correlation filter and is able to help to realize the fast realization by FFT. In order to address the issue of virtual samples in the traditional correlation filter, we have presented the tight correlation filter method to make all of the training samples be selected from the real image region. However, if we still use the circulant assumption by adding a Hanning window to the image region instead of the zero padding and cropping strategy to conduct FFT, the samples near the margin of the image region are heavily affected by the Hanning window and they will decrease the accuracy of filter learning, as Fig. 2 displays. Second, the zero padding and cropping strategy can ensure the feasibility and accuracy of the fast realization based on FFT. According to the convolutional theorem, the circulant convolution can be fast realized by FFT. However, correlation filtering corresponds to linear convolution which cannot be directly realized by FFT, because the image region and the filter do not have the same size, and the dot product in the Fourier domain cannot be conducted. One effective way to address this issue is to convert the linear convolution to circulant convolution by the zero padding strategy. By adding zeros in the margin of both the image region and the filter to make them have the same size, the FFT operation can be executed. Based on the zero padding strategy, linear convolution is equal to the circulant convolution [39]. In addition, the zero padding and cropping strategy can effectively avoid the aliasing problem in circulant convolution without zero padding.

The details of the zero padding and cropping strategy are shown in Fig. 6. As pointed out before, correlation can be considered as linear convolution, which is equal to circulant convolution after padding zeros in the margins of both the image patch and the filter to make them have the same size [39]. According to the Parsevals identity [39], the circulant convolution can be realized by FFT efficiently. As Fig. 6(a) shows, the training region $\mathbf{f}$ is padded by zeros in its edge, generating the augmented $\bar{\mathbf{f}}$ with size $L_v \times L_w$, where $L_v = V + v - 1$ and $L_w = W + w - 1$. Then, $\bar{\mathbf{f}}$ can be transformed into the Fourier domain successfully. The response map $\mathbf{g}$ can be easily extended to the augmented version because the values out of the margin of $\mathbf{g}$ are close to zero based on the Gaussian function. Fig. 6(b) shows how to obtain the final correlation filter. After $\hat{\mathbf{h}}$ is achieved by (3), we can obtain the augmented $\bar{\mathbf{h}}$ by IFFT, in which the aliasing effect can be observed. In practice, the standard filter can be obtained by cropping out the up-left corner region of $\bar{\mathbf{h}}$. The cropping manner is simple but effective and has been successfully used in the image deblurring domain [40]. Thus, we utilize the cropping strategy to avoid complex computation.

Two benefits can be brought by learning in the Fourier domain with the introduced zero padding and cropping strategy and without exploiting the circulant structure. First, the samples corresponding to the zero padding strategy for FFT can be set to be the same size as the target, which can avoid the effect of the background. Second, employing the zero padding strategy for FFT can effectively address the unwanted boundary effects caused by the circulant structure assumption. Because the boundary effects may lead to inaccurate representation and reduce the useful region, using zero padding to alleviate these effects may improve the accuracy of the tracking results.

2) Multichannel Filter: In the aforementioned formulation, we introduce the correlation filtering framework with only a single-channel feature. To improve the representation capability, we would like to extend the single-channel feature to multichannel, for example, HOG, generating several layers of feature planes. Assume the dimension size of the feature at each point is d, then the feature plane in the lth layer can be denoted as $\mathbf{f}^l$, where $l \in \{1, 2, \ldots, d\}$. Correspondingly, as Fig. 7 shows, the multichannel filter banks can be learned according to the multichannel features, similar to [29] and [41]. The objective function in (1) becomes

$$\min_{\mathbf{h}} \left\| \sum_{l=1}^{d} \mathbf{f}^l \otimes \mathbf{h}^l - \mathbf{g} \right\|^2 + \lambda \sum_{l=1}^{d} \left\| \mathbf{h}^l \right\|^2 \qquad (10)$$

where $\mathbf{h}^l$ is the filter in the lth layer of $\mathbf{h}$. Similar to solving (1) and (2), based on the augmented $\bar{\mathbf{f}}^l$ by padding zeros, Parsevals identity, and FFT, the objective function can be rewritten in the Fourier domain

$$\min_{\hat{\mathbf{h}}} \left\| \sum_{l=1}^{d} \hat{\mathbf{f}}^l \odot \hat{\mathbf{h}}^{l*} - \hat{\mathbf{g}} \right\|^2 + \lambda \sum_{l=1}^{d} \left\| \hat{\mathbf{h}}^{l*} \right\|^2 \qquad (11)$$

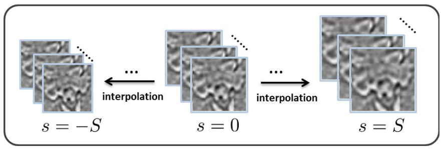

Fig. 8. Generating multiscale filter banks by interpolation.

where $\hat{\mathbf{h}}^l = \mathcal{F}(\bar{\mathbf{h}}^l)$ and $\hat{\mathbf{f}}^l = \mathcal{F}(\bar{\mathbf{f}}^l)$. Then, we can obtain

$$\bar{\mathbf{h}}^l = \mathcal{F}^{-1}\left(\frac{\mathcal{F}\left(\bar{\mathbf{f}}^l\right) \odot \mathcal{F}(\mathbf{g})^*}{\sum_{l=1}^{d} \mathcal{F}\left(\bar{\mathbf{f}}^l\right) \odot \mathcal{F}\left(\bar{\mathbf{f}}^l\right)^* + \lambda}\right). \tag{12}$$

The set $\{\mathbf{h}^l\}_{l=1}^d$ can be cropped from $\{\bar{\mathbf{h}}^l\}_{l=1}^d$, making up the baseline filter bank.

3) Scale Adaptation: Since the obtained correlation filter bank above has a fixed size, it cannot work well when the scale of the target changes heavily. To address the scale variation problem, we further build the correlation filter banks in multiple scales and use a heuristic method to determine the optimal scale and position. Because of the inner spatial structure of the correlation filter, the multiscale filters can be approximately constructed based on the interpolation technology.

Concretely, for each filter layer $\mathbf{h}^l$, we calculate the interpolation planes in multiple scales shown in Fig. 8. Assume the candidate scale set is $\{a^s\}$, where a is the scale base and s is the scale factor with $s \in \{-S, \dots, S\}$. Denote the size of the original filter as $v \times w$, which is the same with the target in the current frame. Then, the size of the filter bank in scale s is $a^s v \times a^s w$. Therefore, the bicubic interpolation is utilized to construct the filter banks in different scales. After the scale augmentation, the final filter banks can be denoted as $\{\mathbf{h}^{sl}\}$ with $s \in \{-S, \dots, S\}$ and $l \in \{1, \dots, d\}$. In practice, the system filter banks used for tracking are acquired based on the frame-by-frame update and interpolation, which is shown in Section IV-C.

B. Tracking and Location

Based on the constructed correlation filter, we conduct tracking and propose a distance importance-based confidence map to determine the location of the target, which not only makes use of the filtering result but also takes the distance importance of the candidate samples into account.

Denote the filter banks from frames $\{1, \dots, t-1\}$ as $\{\mathbf{H}_{t-1}^{sl}\}$. Then, we can complete the tracking in the current frame t. First, we crop the image region in frame t, which centers in the position of the target of frame $t-1$, $\mathbf{p}_{t-1}$, and with width W and height V. In practice, the cropping operation corresponds to sampling the candidate samples in the regression model. Second, dense multichannel features are extracted from the candidate region and a series of feature planes $\{\mathbf{f}'^l\}$ is obtained. Third, $\{\mathbf{f}'^l\}$ and $\{\mathbf{H}_{t-1}^{sl}\}$ are extended to $\{\bar{\mathbf{f}}'^l\}$ and $\{\bar{\mathbf{H}}_{t-1}^{sl}\}$ by padding zeros. Fourth, we apply the filtering operation by employing $\{\bar{\mathbf{H}}_{t-1}^{sl}\}$ in $\{\bar{\mathbf{f}}'^l\}$ separately for $s \in \{-S, \dots, S\}$ in each layer. Then, the response map in scale s is obtained by

$$\mathbf{g}'(s) = \sum_{l=1}^{d} \mathcal{F}^{-1}\left(\mathcal{F}\left(\bar{\mathbf{f}}'^l\right) \odot \mathcal{F}\left(\bar{\mathbf{H}}_{t-1}^{sl}\right)^*\right)/a^{2s} \tag{13}$$

where a^{2s} is used to normalize the response values in different scales.

As we have pointed out above, each point in the confidence map corresponds to a unique candidate sample. It should be noted that the importance of the candidate samples is different. It is assumed that the target cannot move too far in the consecutive frames, so that the sample closer to the tracking result in the last frame should be assigned to a larger importance weight while the one which is farther away should have a smaller weight. Therefore, we further calculate the importance weight map $\mathbf{d}$ of candidate samples by the Gaussian function

$$d(\mathbf{p}) = \exp\left(\left(-\|\mathbf{p} - \mathbf{p}_{t-1}\|^2\right)/\sigma_d^2\right) \tag{14}$$

where $\mathbf{p}$ denotes the position of the candidate sample, $\mathbf{p}_{t-1}$ is the position of the tracking result in the last frame, $d(\mathbf{p})$ is the weight element of $\mathbf{d}$ corresponding to the position $\mathbf{p}$, and σ_d^2 is the weight parameter. By embedding the weight map into the confidence map in (13), we can obtain the final confidence map

$$\mathbf{g}''(s) = \mathbf{g}'(s) \odot \mathbf{d}. \tag{15}$$

Because the response map $\mathbf{g}''$ is cubic based on a position vector $\mathbf{p}$ and a scale variable s, we search for the maximum response value over the whole position and scale space to locate the target

$$\left(\mathbf{p}_t, s_{\text{opt}}\right) = \arg\max_{(\mathbf{p}, s)} \mathbf{g}'' \tag{16}$$

where $\mathbf{p}_t$ and s_{opt} represent the predicted optimal position and scale of the target, respectively, and $\{(\mathbf{p}, s)\}$ represents the candidate position and scale space.

C. Update

To cope with the appearance changes of the target during tracking, the correlation filter banks should be updated once the tracking result is obtained. Therefore, we adopt an incremental update strategy. Assume the multichannel filter banks in frame $t-1(t>1)$ are $\{\mathbf{H}_{t-1}^{sl}\}$, where $\mathbf{H}_1^{0l} = \mathbf{h}_1^l$ and $\mathbf{H}_1^{sl}(s \neq 0)$ is obtained by interpolation. Once the tracking result in frame t is obtained, we can learn a new correlation filter bank $\{\mathbf{h}_t^l\}$ in frame t with the new tracking result according to the determined position and the scale of the target, and then utilize it to update $\{\mathbf{H}_{t-1}^{sl}\}$. Since $\{\mathbf{h}_t^l\}$ is learned in the optimal scale in the current frame, we resize $\{\mathbf{H}_{t-1}^{0l}\}$ to make it fit the same scale first. Assuming that the learning rate is θ, the updated filter bank $\{\mathbf{H}_t^{0l}\}$ can be obtained by the linear combination of $\{\mathbf{H}_{t-1}^{0l}\}$ and $\{\mathbf{h}_t^l\}$

$$\mathbf{H}_t^{0l} = (1-\theta)\mathbf{H}_{t-1}^{0l} + \theta \mathbf{h}_t^l, \quad l = 1, \dots, d. \tag{17}$$

Then, the filter banks $\{\mathbf{H}_t^{sl}\}$ in other scales can be obtained by interpolation as well, used for filtering and detection in frame $t+1$. The iteration process is summarized in Algorithm 1.

Algorithm 1 SCFR Tracking: Iteration in Frame t

```
Input:
    Frame $I_t$; Previous object position $\mathbf{p}_{t-1}$ and size $v \times w$; Filter banks $\{\mathbf{H}_{t-1}^{sl}\}$.
Output:
    Object position $\mathbf{p}_t$ and updated size $v \times w$; Updated filter banks $\{\mathbf{H}_t^{sl}\}$.
Filtering and Tracking.
    (1) Crop the candidate image patch at $\mathbf{p}_{t-1}$ from $I_t$ and extract the multichannel features $\{\mathbf{f}'^{l}\}$;
    (2) Augment $\{\mathbf{f}'^{l}\}$ and $\{\mathbf{H}_{t-1}^{sl}\}$ by padding zeros;
    (3) Calculate the distance weighed response $\mathbf{g}''(s)$ by Eqn. 13, Eqn. 14 and Eqn. 15;
    (4) Determine the optimal position $\mathbf{p}_t$ and scale $s_{\mathrm{opt}}$ by Eqn. 16;
    (5) Determine the object size by $a^{s_{\mathrm{opt}}}v \times a^{s_{\mathrm{opt}}}w$.
Learning and Update.
    (1) Crop the training patch at $\mathbf{p}_t$ from $I_t$, and extract and augment the multichannel features $\{\mathbf{f}^{l}\}$;
    (2) Learn the filter bank $\{\mathbf{h}_t^{l}\}$ in $I_t$ by Eqn. 12;
    (3) Resize the filter bank $\{\mathbf{H}_{t-1}^{0l}\}$ to scale $s_{\mathrm{opt}}$, and updated $\{\mathbf{H}_t^{0l}\}$ by Eqn. 17;
    (4) Generate $\{\mathbf{H}_t^{sl}\}$ in other scales ($s \neq 0$) by interpolation.
```

V. Experiments

A. Experimental Setup

The configuration of our tracker is as follows. Since the HOG feature [42] with 5-pixel window size and 9 orientations obtains excellent performance on object detection and tracking in many methods [16], [43], [44], it is adopted as the multichannel feature and is densely sampled in our method. The sizes of the cropped regions for training and detection are experimentally set to 3 times the target size and adaptively adjusted, since a larger region size will significantly increase the computation complexity while a smaller size may not capture the target when it moves fast. The tradeoff parameter λ is set as 0.01, which is used to balance the regression errors and the regularization term. In practice, the appearance model is not sensitive to λ. If the parameter satisfies that λ is smaller than 0.02 and larger than 0, we can get almost the same tracking performance. The Gaussian response function used to determine the filtering result as well as the regression value is experimentally set with $\sigma^2 = 0.03$. A smaller σ^2 can provide better discriminability, but will bring bigger regression errors. The learning rate is critical to learn the changes of the appearance timely. A larger learning rate can make the model more robust to deformation but will accumulate the representation errors when the occlusions exist. Conversely, a smaller learning rate may not learn the deformation changes but is more robust to occlusions. Thus, the learning rate θ is set to 0.025, which is used to balance the deformation learning and occlusion handling. To realize scale adaption, 5 scales are used with $a = 1.03$ and $S = 2$. More scales with smaller a and larger S will get better scale adaption but will greatly increase the computation complexity, and fewer scales with larger a and smaller S will lead to inaccurate scale adaption. The Gaussian function used to calculate the distance importance weight is set with $\sigma_d^2 = 7$, which is experimentally determined by balancing the filtering result and the influence of the distance. A larger σ_d^2 may make the tracker less robust to similar distractors while a smaller σ_d^2 will decrease the accuracy of the filtering result. All parameters are fixed on the experiments.

TABLE I
Comparison Results of Average CLE (in Pixel), Average VOR, Precision ($\mathrm{Th}_p = 20$), and SR ($\mathrm{Th}_s = 0.5$) Results of SCFR and the 11 Famous Trackers in the OTB2013

Method	Average CLE	Average VOR	Precision (20)	SR (0.5)
SCFR	29.3	0.622	0.835	0.764
ECO	17.2	0.710	0.913	0.870
ADNet	14.5	0.661	0.892	0.824
MDNet	8.2	0.710	0.932	0.896
MEEM	24.2	0.566	0.806	0.699
Struck	50.7	0.476	0.654	0.557
SCM	54.2	0.505	0.648	0.615
ASLA	73.2	0.438	0.530	0.509
CXT	68.6	0.427	0.570	0.487
TLD	48.4	0.438	0.601	0.515
VTD	47.6	0.420	0.583	0.498
VTS	51.0	0.420	0.582	0.501

Four criteria are used to evaluate the performance of the tracker. The first is the average center location error (CLE), which is defined as the average of the errors of the obtained target center position and the ground truth. The second is precision, which is computed by the ratio of the number of frames whose CLE is smaller than a threshold Th_p and the number of total frames. The third is the average Pascal VOC overlap rate (VOR). VOR is defined as the average of $\mathrm{Score} = ([\mathrm{area}(R_S \cap R_G)]/[\mathrm{area}(R_S \cup R_G)])$, where R_S and R_G represent the rectangles of the tracking result and ground truth in one frame, respectively [45]. The fourth is success rate (SR). If the VOR in a frame is larger than a predefined threshold Th_s, the tracking is considered successful in that frame. Then, SR is defined as the ratio of the number of success frames and the total frames. By assigning different values to Th_p and Th_s, the precision plots and success plots can be obtained to demonstrate the overall performance of the tracker. Moreover, the area under the curve can be used as the evaluation criterion as well.

B. Comparison With State-of-the-Art Trackers on OTB2013

Denoting the proposed scale-adaptive correlation filter and ridge regression-based tracker as SCFR, then we evaluate its performance in the OTB2013 dataset and compare it with the top several trackers in the ranking list of the OTB2013 [3], including structured output tracking with kernels (Struck) [14], tracker by sparsity-based collaborative model (SCM) [23], tracking-learning-detection (TLD) [46], tracker with adaptive structural local sparse appearance model (ASLA) [47], context tracker (CXT) [48], visual tracking decomposition (VTD) [49], and visual tracker sampler (VTS) [50], and some recent famous trackers efficient convolution operators for tracking (ECO) [34], action-decision networks for visual tracking (ADNet) [51], multidomain convolutional neural networks for visual tracking (MDNet) [52], and tracking via multiple experts using entropy minimization (MEEM) [44].

First, we compare the overall performance of the competing trackers on all 51 sequences. Table I shows the comparison results on average CLE, average VOR, precision ($\mathrm{Th}_p = 20$ pixels), and SR ($\mathrm{Th}_s = 0.5$) of our method and the competing

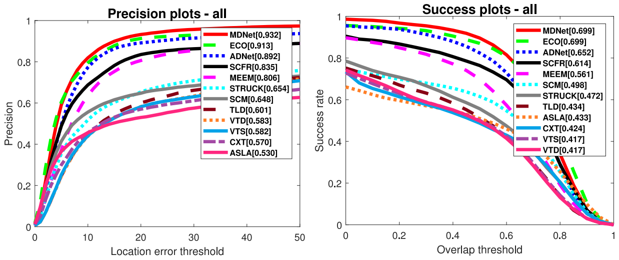

Fig. 9. Precision plots and success plots of SCFR and the competing trackers on all 51 sequences in OTB2013. The precision at $\text{Th}_p = 20$ pixels and the AUC score are put in the bracket behind the name of the tracker.

trackers. From Table I, we can find that our SCFR method achieves the desirable results on all 4 criteria. The average CLE of SCFR is 29.3 pixels, which is larger than ECO, ADNet, MDNet, and MEEM, but smaller than the remaining competing trackers. The average VOR of SCFR is 0.622, which is only lower than ECO, ADNet, and MDNet, and is better than many other trackers as well. For the competing trackers, Struck and SCM obtain the best precision and SR results, respectively, in the OTB2013 list. However, the precision with $\text{Th}_p = 20$ pixels of SCFR is 0.835, which outperforms Struck by 18%. Besides, SCFR also outperforms SCM by about 15% in SR. Moreover, since the ECO, ADNet, and MDNet methods use the convolutional neural network-based features to improve the representation capability while the remaining trackers only use the traditional handcrafted features, they perform better than the others. Our SCFR method is interior to ECO, ADNet, and MDNet, but outperforms all of the remaining trackers without deep features. The precision plots and the success plots are shown in Fig. 9, which shows the average precision and SR on all 51 sequences under different thresholds. It can be observed that the performance of SCFR is better than most existing state-of-the-art trackers without deep features in the OTB2013 dataset as well.

Next, we evaluate the performance of the trackers under different conditions by the results on the sequences with different attributes. The average precision plots and success plots are illustrated in Fig. 10, from which we can find that our SCFR acquires better performance than many trackers in most conditions, including occlusion, deformation, scale variation, background clutter, etc. Therefore, we explain the mechanism that makes SCFR achieve good performance.

Occlusions: Fig. 10(a) shows the precision plots and success plots of the competing trackers on 29 sequences in the condition of occlusions. It can be observed that when $\text{Th}_p = 20$ pixels and $\text{Th}_s = 0.5$, SCFR outperforms SCM which performs best among the competing trackers in the OTB2013 ranking list by more than 10% on both precision and SR, and is only weaker than ECO, ADNet, MDNet, and MEEM. As mentioned before, SCFR follows the tracking-by-detection framework, and it has better discriminability to the background including occlusions. Besides, the multichannel feature is extracted pixel wise, and the HOG feature works in the local manner. Thus, SCFR is robust to partial occlusions.

Deformations: Fig. 10(b) gives the precision plots and success plots of the competing trackers on 19 sequences with deformations. It can be seen that the plots obtained by SCFR are much better than many other methods. This is because the earned correlation filter can build an accurate appearance model and the online update model can adapt to the deformation of the object to retain the accuracy of the appearance model, which makes SCFR have a desirable expression in the condition of deformation.

Out-of-Plane Variations: The comparison results of precision plots and success plots of the competing trackers in the condition of out-of-plane variations are displayed in Fig. 10(c). We can find that both of these plots achieved by SCFR significantly outperform most of the others. On one hand, the filter-based appearance model can provide finer discriminability. On the other hand, the incremental update strategy can learn that the appearance changes timely.

Scale Variations: Fig. 10(d) demonstrates the precision plots and success plots of the competing trackers on 28 sequences with scale variations. Our SCFR also has significant advantages, and it ranks fourth on both plots. A highlight of SCFR is that it utilizes a multiscale strategy based on interpolation to deal with the scale changes of the object. By the precision and success plots on the sequences with scale attributes, we can find that the proposed scale-adaptive correlation filter works well and outperforms SCM and ASLA which employ particle filters to address scale variations.

Fast Motion: The precision plots and success plots in Fig. 10(g) demonstrate that SCFR can acquire robust results when the objects move fast. In our formulation, we utilize the bounding box with the same size as the target for representation, which can effectively deal with the background changes caused by fast motion. Combined with the filter-based appearance model, SCFR performs well when the objects move fast.

Background Clutter: As the comparison results in Fig. 10(h) display, in the condition of background clutter, SCFR achieves the sixth best results. Since the filter exploits the relations of the target and the background, it provides a more accurate appearance model which has finer discriminability. Therefore, SCFR works well when there is background clutter.

C. Comparison With Other Correlation Filter-Based Trackers

We also compare the performance of our tracker with the related filter-based tracking methods, including KCF [16], CSK [15], CN [32], STC [37], DSST [17], and SAMF [18], all of which have publicly available codes. Different from the above trackers mentioned in Section II, SCFR models tracking from the signal detection perspective and accords with the tracking-by-detection framework. The correlation filter in our method is learned with the same size as the target, which can alleviate the effect of the fast-changing background and does not need the circulant structure assumption for FFT. The SCFR method can address the scale variations adaptively by building multiscale filter banks.

Fig. 11 illustrates the evaluation of the overall performance of these trackers. For the precision plots, SCFR, KCF, SAMF, and DSST have similar performance and significantly

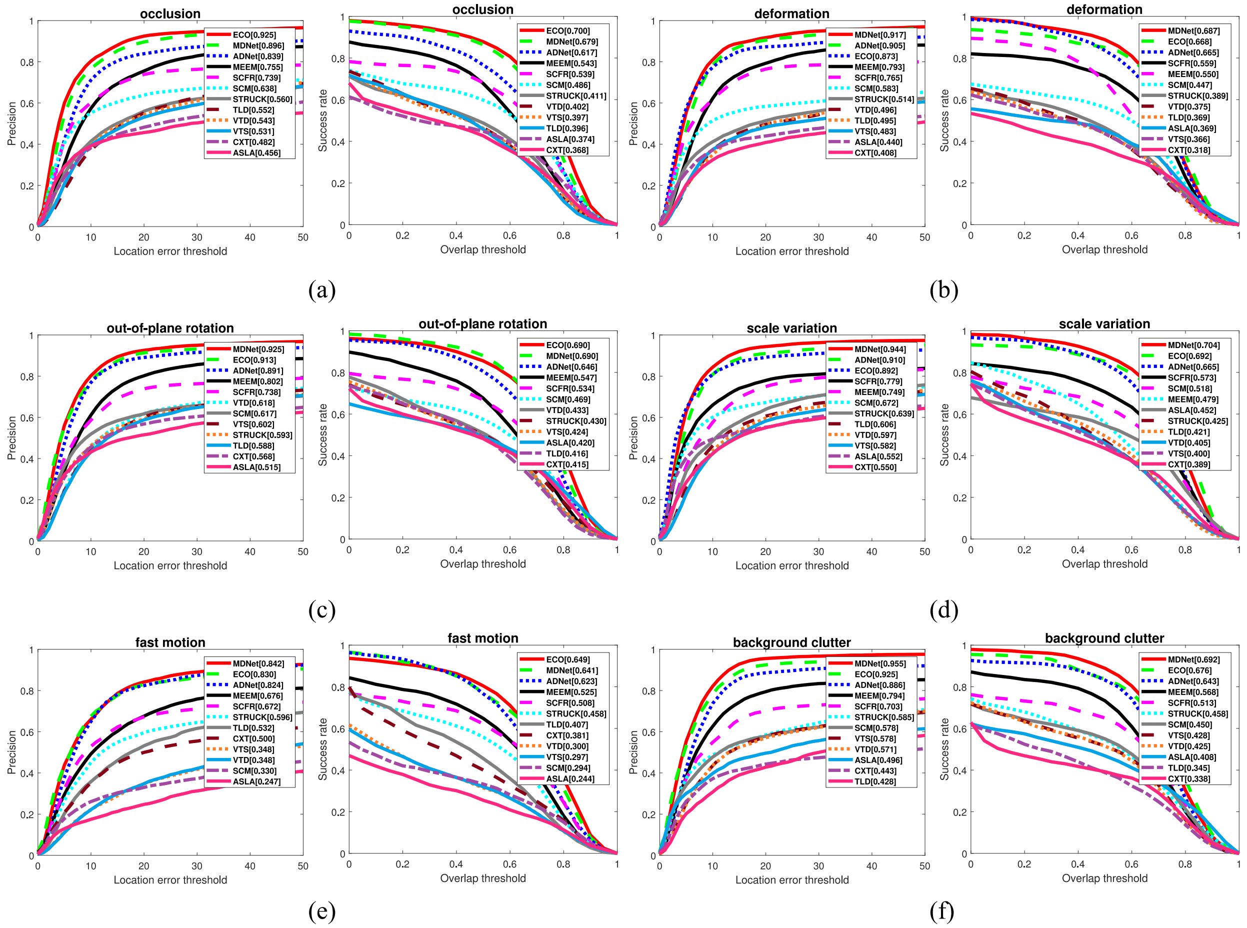

(a) (b) (c) (d) (e) (f)

Fig. 10. Precision plots and success plots of SCFR and the competing trackers on the sequences with different attributes. The number in parenthesis represents the amount of the sequences with the corresponding attribute. Precision and success plots of (a) occlusion attribute, (b) deformation attribute, (c) out-of-plane rotation attribute, (d) scale variation attribute, (e) fast motion attribute, and (f) background clutter attribute.

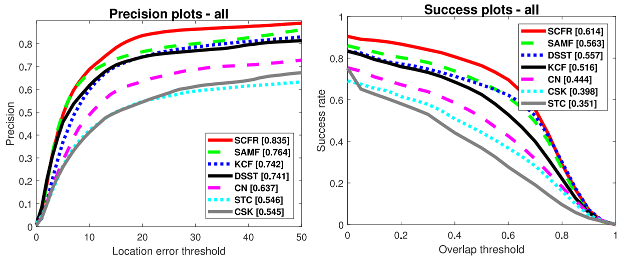

Fig. 11. Precision plots and success plots of SCFR and the filter-based trackers on all the 51 sequences in OTB2013 (Precision with $\text{Th}_p = 20$ pixels and AUC score are shown in brackets).

outperform the rest trackers. Moreover, for the success plots, SAMF and DSST with scale adaption perform better than the trackers using fixed-size bounding boxes for representation. However, SCFR has better performance than SAMF and DSST. In practice, this benefits much from the success in the condition of scale variation and fast motion. On one hand, the proposed multiscale strategy in the filter domain can adaptively handle the scale variation issue, which expresses better than the scale adaption in image domain of SAMF and DSST. On the other hand, the bounding box with the same size as the target can well exclude the influence of the fast-changing background.

As Fig. 12(a) shows that because of the proposed scale adaption module, SCFR significantly outperforms the other trackers on both the average precision plots and average success plots of all 28 sequences with scale changes. For the competing trackers, KCF, CN, and CSK all make use of the fixed-size bounding box for representation, while STC, SAMF, and DSST use different scale adaption strategies. We can see that the scale adaption module of SCFR works well. Fig. 12(b) demonstrates the comparison results in the condition of fast motion. It can be observed that SCFR performs much better than the other methods, which exhibits that setting the bounding box to be the same size as the target can effectively decrease the distraction from the background. Most of the competing trackers employ a much larger bounding box for representation to satisfy the circulant structure assumption, which may be more easily affected by the fast-changing background.

D. Analysis of Multiscale Filters

To address the scale adaption issue, we propose the multiscale filter banks by making use of the spatial structure and interpolation. Besides, we set the parameter corresponding to the number of scales as 5, which means the multiscale filter

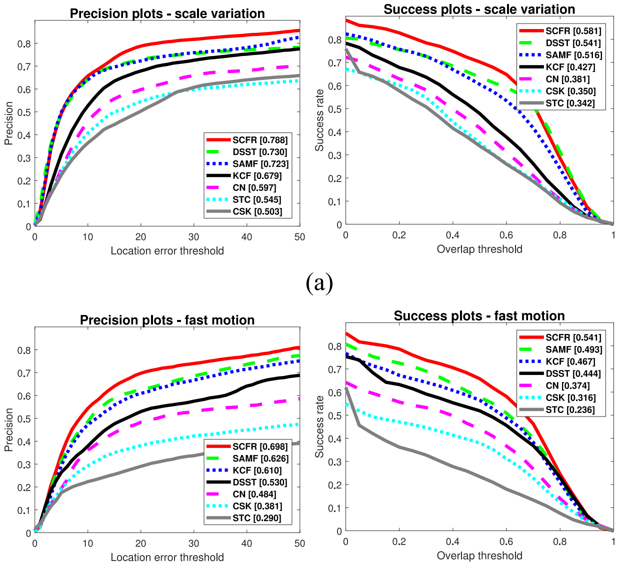

(a)

(b)

Fig. 12. Precision plots and success plots of SCFR and the filter-based trackers on all 51 sequences (precision with $\mathrm{Th}_p = 20$ pixels and the AUC score are shown in brackets). Precision and success plots of (a) scale variation attribute and (b) fast motion attribute.

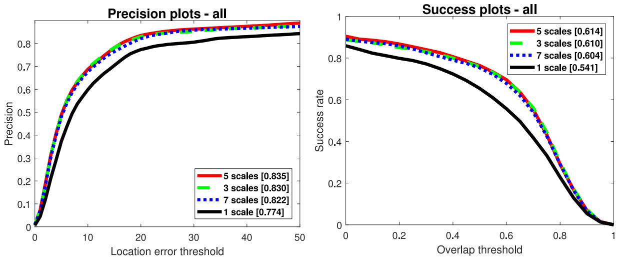

Fig. 13. Precision plots and success plots of the SCFR trackers with different scales in OTB2013.

banks are generated by 5 scales. Therefore, to better explore the impact of the multiscale filter banks, we construct another 3 trackers with the multiscale filters in different scales, including 7 scales, 3 scales, and 1 scale. Note that the tracker with only 1 scale corresponds to the tracker without scale adaption.

We run these trackers in the OTB2013 dataset and the comparison results are displayed in Fig. 13. It can be found that when 5 scales are utilized, the SCFR tracker can get the best precision plot and success plot. We can also observe that the trackers with 3 scales and 7 scales express some weaker than the tracker with 5 scales. For example, the tracker with 5 scales outperforms that with 7 scales by about 1% on both precision and AUC score. Specifically, when compared with the tracker without multiscale filter banks, the tracker with 5 scales has significant advantages. Specifically, the tracker with 5 scales outperforms the tracker with only 1 scale and without scale adaption by about 6% and 7% on the precision and AUC score, respectively, indicating that the multiscale filter banks can effectively improve tracking performance by dealing with the scale variation problem. Commonly, the performance of the tracker with more scales can get better tracking results in theory, which can better deal with the scale change problem. However, the filter banks with more scales will cost more time.

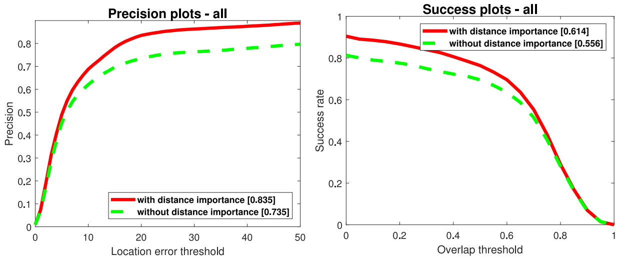

Fig. 14. Precision plots and success plots of the SCFR trackers with and without distance importance weight in OTB2013.

In addition, the tracker with more than 5 scales can more easily be affected by other challenging factors.

E. Analysis of Distance Importance-Based Confidence Map

To locate the target in the new frame, we propose a novel distance importance-based confidence map calculation model in our method. Besides the tracking result used in other correlation filter-based tracking methods, the importance of the candidate samples is considered and embedded into the confidence map by the filtering in our approach. In other words, the final tracking result is determined by both the distance importance and the filtering result. Therefore, we investigate the effect of the distance importance strategy in the motion model.

We construct a new tracker which only uses the filtering result without the distance importance map to determine the location. We compare the new tracker without importance weight with the standard SCFR which retains the distance importance module in the OTB2013 dataset. The comparison results are shown in Fig. 14, from which we can observe that performance of the tracker with distance importance significantly outperforms that without distance importance. Note that the precisions of the tracker without distance importance are 0.735 and 0.558, which are about 10% and 6% lower than that with distance importance. This indicates that the performance of the tracker is greatly improved by considering the distance importance. In practice, during the tracking process, there exist many similar distractors which may make the tracking drift. However, by calculating the confidence map weighted by the distance importance, the impact caused by the similar distractors which are far away from the target can be effectively alleviated, and the tracking performance can be improved.

F. Evaluation in More Datasets

Besides the OTB2013 dataset in which the SCFR tracker has achieved good results, we also evaluate the performance of our SCFR tracker in more datasets, including the OTB-100 dataset [53] and VOT2016 dataset [54], to explore the effect of the settings of the tracker.

Evaluation in the OTB-100 Dataset: We further evaluate the performance of SCFR in the OTB-100 dataset which is the extension version of OTB2013. Besides the original sequences in OTB2013, more sequences are added up to 100 in the OTB-100 dataset. Therefore, we compare SCFR with several famous tracking methods, including ECO [34], MDNet [52],

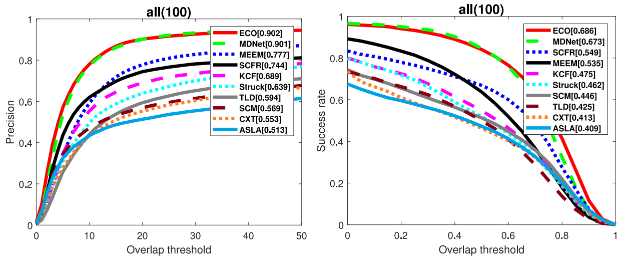

Fig. 15. Precision plots and success plots of SCFR and the competing trackers in the OTB-100 dataset.

ADNet [51], ASLA [47], SCM [23], locally orderless tracking [55], CSK [15], CXT [48], OAB [20], multitask sparse learning tracking [56], color-based probabilistic tracking [57], local sparse appearance model and K-selection tracking [58], Kernel MeanShift [59], and the multiple instance learning tracker (MIL) [11] in this dataset. The comparison results of precision plots and success plots are shown in Fig. 15, from which we can obtain the similar conclusion with that in OTB2013. It can be observed that the precision at $\mathrm{Th}_p = 20$ pixels obtained by SCFR is 0.744 and the AUC score is 0.549, which ranks fourth and third, respectively. It can be found that the trackers with deep features also perform better than the others, but SCFR almost outperforms all of the trackers without deep features. The overall performance of SCFR is similar to MEEM, worse than ECO and MDNet, and better than the remaining trackers.

Evaluation in the VOT2016 Dataset: We also evaluate our SCRF method in the VOT2016 dataset. There are 65 sequences in the VOT2016 dataset, which captures deformations, occlusions, illumination changes, abrupt motion changes, etc. Specifically, the VOT framework uses two weakly correlated metrics, the accuracy and the robustness, for a standardized analysis, where the accuracy is defined as the average bounding box overlap and the robustness denotes the number of reinitializations. The evaluation is conducted by ranking analysis based on these two criteria. Hereby, we compare our SCFR method with 18 famous tracking methods, including the scale-and-state aware tracker, multilevel deep feature tracker, correlation filters with convolutional features tracker extended with response information failure detection, best displacement flow [60], scalable kernel correlation filter with sparse feature integration [61], dynamic feature selection tracker [62], optical-flow clustering tracker, DSST [17], adaptive color tracker [63], MDNet-N, guided correlation filter, anchor template tracker, transfer learning-based visual tracking with Gaussian processes regression [64], adaptive regression target DSST, MIL [11], DFT [65], incremental learning for robust visual tracking [5], and the anchor template tracker (NCC) [66] in the VOT2016 dataset, and show the comparison results in Table II following the evaluation framework of VOT. The comparison results are obtained in baseline manner with initialization in the ground truth. From Table II, we can find that the average ranking of our SCFR tracker is 3.8 on accuracy which outperforms many competing trackers. SCFR acquires the robustness ranking 8.52 and expected overlap 0.1722, both of which rank in the middle among the trackers. Specifically, the ranking in accuracy of SCFR is higher than that in robustness, which guides us to improve the robustness of SCFR in the future.

TABLE II
COMPARISON RESULTS ON VOT2016

Method	Accuracy	Robustness	Expected overlap
SCFR	3.8	8.52	0.1722
SSAT	1.53	3.3	0.3207
MLDF	3.83	2.4	0.3106
RFD-CF2	4.02	3.57	0.2415
BDF	8.68	8.88	0.1361
sKCF	4.37	9.1	0.1533
DFST	4.33	8.07	0.1513
FCT	8.27	8.95	0.1412
DSST	3.53	6.9	0.1814
ACT	5.45	6.78	0.1726
MDNet-N	2.08	3.57	0.2572
GCF	2.75	5.1	0.2179
ANT	4.67	6.57	0.2045
TGPR	4.93	7.02	0.1811
ART-DSST	3.82	7	0.1673
MIL	6.97	9.18	0.1645
DFT	5.13	10.82	0.1395
IVT	7.22	11.55	0.1147
NCC	4.68	15.35	0.0804

G. Limitations

As mentioned above, SCFR acquires good precision and SR results in the benchmark datasets, especially in the conditions of scale variations and fast motions. However, we should note that SCFR fails on some very challenging sequences, by which we analyze the limitations of SCFR.

Fig. 16 demonstrates three failure examples on some representative sequences. On *ironman*, the target moves so fast, together with heavy deformation, illumination variation, and scale changes, that tracking begins to drift in the early stage (e.g., in Frame 28). On one hand, the fast, heavy deformation of consecutive frames makes the learned filters quite different, which will degrade the robustness of the appearance model by incremental learning. On the other hand, the degree of the scale changes exceeds the predefined range, which will affect the location precision as well. The same issue occurs on *matrix* where SCFR also drifts. Under these complex challenging conditions, a more powerful appearance model should be designed to improve the representation ability, and the learning rate should be adjusted adaptively. On *lemming*, heavy occlusion lasts for a long time, which accumulates the errors of the learned appearance model. To handle the issue of long-term full occlusions, the occlusion judging strategy and motion prediction model can be considered to improve the tracking performance.

In our MATLAB platform on PC with an Intel i7 CPU 3.4 GHz, the running speed of our standard SCFR tracker is 2.0 frames/s, and the speed of the tracker without scale adaption is 9.1 frames/s, both of which are faster than MDNet, SCM, ALSA, VTD, VTS, etc., but slower than ECO, MEEM, KCF, Struck, TLD, etc. Although SCFR has not achieved real-time performance up to now, we can speed it up by employing parallel strategy in several modules of the model in the future. On one hand, because the multiscale filters are implemented by

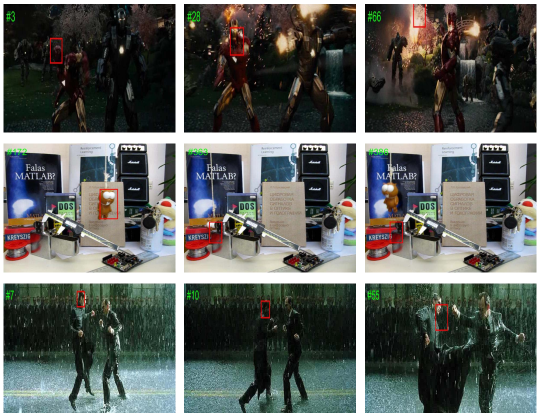

Fig. 16. Failure cases of SCFR. Top to down: *ironman*, *lemming*, and *matrix*.

interpolation and used to realize the tracking separately, they can work in a parallel manner and each filter can be set in a single thread which can reduce the running time to only about $1/S$ times of the original filter banks' cost time, where S is the number of scales. On the other hand, the computation on the multichannel features can also be divided into single channels. By assigning a work thread to each channel and conducting the FFT operation on all channels at the same time, the running speed of SCFR can be further improved. Because the parallel strategy does not decrease the tracking accuracy, it may be a feasible and effective way to improve the tracking speed of SCFR.

VI. Conclusion

In this paper, we propose a novel tracking method based on the correlation filtering formulation as well as ridge regression formulation. From the signal detection perspective, the relations of the neighboring sample patches are fully exploited and a tight correlation filter is learned to represent the tracker without the circulant structure assumption. By making use of the spatial structure of the filter, the multiscale filter banks can be implemented to handle the challenging scale variation problem adaptively. Moreover, a distance importance-based confidence calculation model is presented to determine the final tracking result. Experimental results demonstrate that the proposed method can outperform many state-of-the-art trackers in the benchmark datasets. Further, we would like to introduce deep features for better tracking performance and improve the running speed of our tracker to satisfy practical applications.

References

[1] A. Yilmaz, O. Javed, and M. Shah, "Object tracking: A survey," *ACM Comput. Surveys*, vol. 38, no. 4, p. 13, 2006.

[2] H. Yang, L. Shao, F. Zheng, L. Wang, and Z. Song, "Recent advances and trends in visual tracking: A review," *Neurocomputing*, vol. 74, no. 18, pp. 3823–3831, 2011.

[3] Y. Wu, J. Lim, and M.-H. Yang, "Online object tracking: A benchmark," in *Proc. IEEE Conf. Comput. Vis. Pattern Recognit.*, 2013, pp. 2411–2418.

[4] X. Mei and H. Ling, "Robust visual tracking using l1 minimization," in *Proc. IEEE Conf. Int Comput. Vis.*, Oct. 2009, pp. 1436–1443.

[5] D. Ross, J. Lim, R. Lin, and M. Yang, "Incremental learning for robust visual tracking," *Int. J. Comput. Vis.*, vol. 77, no. 1, pp. 125–141, 2008.

[6] H. Li, C. Shen, and Q. Shi, "Real-time visual tracking using compressive sensing," in *Proc. IEEE Conf. Comput. Vis. Pattern Recognit.*, 2011, pp. 1305–1312.

[7] Z. Chen, X. You, B. Zhong, J. Li, and D. Tao, "Dynamically modulated mask sparse tracking," *IEEE Trans. Cybern.*, vol. 47, no. 11, pp. 3706–3718, Nov. 2017.

[8] Y. Yang, W. Hu, Y. Xie, W. Zhang, and T. Zhang, "Temporal restricted visual tracking via reverse-low-rank sparse learning," *IEEE Trans. Cybern.*, vol. 47, no. 2, pp. 485–498, Feb. 2017.

[9] Z. He, S. Yi, Y.-M. Cheung, X. You, and Y. Y. Tang, "Robust object tracking via key patch sparse representation," *IEEE Trans. Cybern.*, vol. 47, no. 2, pp. 354–364, Feb. 2017.

[10] S. Avidan, "Support vector tracking," *IEEE Trans. Pattern Anal. Mach. Intell.*, vol. 26, no. 8, pp. 1064–1072, Aug. 2004.

[11] B. Babenko, M.-H. Yang, and S. Belongie, "Robust object tracking with online multiple instance learning," *IEEE Trans. Pattern Anal. Mach. Intell.*, vol. 33, no. 8, pp. 1619–1632, Aug. 2011.

[12] S. Zhang, X. Yu, Y. Sui, S. Zhao, and L. Zhang, "Object tracking with multi-view support vector machines," *IEEE Trans. Multimedia*, vol. 17, no. 3, pp. 265–278, Mar. 2015.

[13] Q. Liu, J. Yang, K. Zhang, and Y. Wu, "Adaptive compressive tracking via online vector boosting feature selection," *IEEE Trans. Cybern.*, vol. 47, no. 12, pp. 4289–4301, Dec. 2017.

[14] S. Hare, A. Saffari, and P. H. S. Torr, "Struck: Structured output tracking with kernels," in *Proc. Conf. IEEE Int Comput. Vis.*, 2011, pp. 263–270.

[15] J. A. F. Henriques, R. Caseiro, P. Martins, and J. Batista, "Exploiting the circulant structure of tracking-by-detection with kernels," in *Proc. Eur. Conf. Comput. Vis.*, 2012, pp. 702–715.

[16] J. F. Henriques, R. Caseiro, P. Martins, and J. Batista, "High-speed tracking with kernelized correlation filters," *IEEE Trans. Pattern Anal. Mach. Intell.*, vol. 37, no. 3, pp. 583–596, Mar. 2015.

[17] M. Danelljan, G. Häger, F. S. Khan, and M. Felsberg, "Accurate scale estimation for robust visual tracking," in *Proc. Brit. Mach. Vis. Conf.*, 2014, pp. 1–11.

[18] Y. Li and J. Zhu, "A scale adaptive kernel correlation filter tracker with feature integration," in *Proc. Eur. Conf. Comput. Vis. Workshops*, 2014, pp. 254–265.

[19] S. Avidan, "Ensemble tracking," *IEEE Trans. Pattern Anal. Mach. Intell.*, vol. 29, no. 2, pp. 261–271, Feb. 2007.

[20] H. Grabner, M. Grabner, and H. Bischof, "Real-time tracking via on-line boosting," in *Proc. Brit. Mach. Vis. Conf.*, vol. 1, 2006, pp. 47–56.

[21] F. Tang, S. Brennan, Q. Zhao, and H. Tao, "Co-tracking using semi-supervised support vector machines," in *Proc. IEEE Int. Conf. Comput. Vis.*, 2007, pp. 1–8.

[22] K. Zhang, L. Zhang, and M.-H. Yang, "Real-time compressive tracking," in *Proc. Eur. Conf. Comput. Vis.*, 2012, pp. 864–877.

[23] W. Zhong, H. Lu, and M.-H. Yang, "Robust object tracking via sparsity-based collaborative model," in *Proc. IEEE Conf. Comput. Vis. Pattern Recognit.*, 2012, pp. 1838–1845.

[24] X. Li, A. Dick, C. Shen, A. van den Hengel, and H. Wang, "Incremental learning of 3D-DCT compact representations for robust visual tracking," *IEEE Trans. Pattern Anal. Mach. Intell.*, vol. 35, no. 4, pp. 863–881, Apr. 2013.

[25] H. Possegger, T. Mauthner, and H. Bischof, "In defense of color-based model-free tracking," in *Proc. IEEE Conf. Comput. Vis. Pattern Recognit.*, 2015, pp. 2113–2120.

[26] Q. Wang, J. Fang, and Y. Yuan, "Multi-cue based tracking," *Neurocomputing*, vol. 131, pp. 227–236, May 2014. [Online]. Available: http://www.sciencedirect.com/science/article/pii/S0925231213010801

[27] J. Fang, Q. Wang, and Y. Yuan, "Part-based online tracking with geometry constraint and attention selection," *IEEE Trans. Circuits Syst. Video Technol.*, vol. 24, no. 5, pp. 854–864, May 2014.

[28] J. Fang, H. Xu, Q. Wang, and T. Wu, "Online hash tracking with spatio-temporal saliency auxiliary," *Comput. Vis. Image Understanding*, vol. 160, pp. 57–72, Jul. 2017. [Online]. Available: http://www.sciencedirect.com/science/article/pii/S1077314217300565

[29] V. N. Boddeti, T. Kanade, and B. V. K. V. Kumar, "Correlation filters for object alignment," in *Proc. IEEE Conf. Comput. Vis. Pattern Recognit.*, Jun. 2013, pp. 2291–2298.

[30] A. Rodriguez, V. N. Boddeti, B. V. Kumar, and A. Mahalanobis, "Maximum margin correlation filter: A new approach for localization and classification," *IEEE Trans. Image Process.*, vol. 22, no. 2, pp. 631–643, Feb. 2013.

[31] D. S. Bolme, J. R. Beveridge, B. A. Draper, and Y. M. Lui, "Visual object tracking using adaptive correlation filters," in *Proc. IEEE Conf. Comput. Vis. Pattern Recognit.*, 2010, pp. 2544–2550.

[32] M. Danelljan, F. S. Khan, M. Felsberg, and J. V. D. Weijer, "Adaptive color attributes for real-time visual tracking," in *Proc. IEEE Conf. Comput. Vis. Pattern Recognit.*, 2014, pp. 1090–1097.

[33] C. Ma, J.-B. Huang, X. Yang, and M.-H. Yang, "Hierarchical convolutional features for visual tracking," in *Proc. IEEE Int. Conf. Comput. Vis.*, 2015, pp. 3074–3082.

[34] M. Danelljan, G. Bhat, F. S. Khan, and M. Felsberg, "ECO: Efficient convolution operators for tracking," in *Proc. IEEE Conf. Comput. Vis. Pattern Recognit.*, Jul. 2017, pp. 6931–6939.

[35] M. Mueller, N. Smith, and B. Ghanem, "Context-aware correlation filter tracking," in *Proc. IEEE Conf. Comput. Vis. Pattern Recognit.*, 2017, pp. 1396–1404.

[36] Z. He, Y. Fan, J. Zhuang, Y. Dong, and H. Bai, "Correlation filters with weighted convolution responses," in *Proc. IEEE Conf. Comput. Vis. Pattern Recognit.*, 2017, pp. 1992–2000.

[37] K. Zhang, L. Zhang, Q. Liu, D. Zhang, and M.-H. Yang, "Fast visual tracking via dense spatio-temporal context learning," in *Proc. Eur. Conf. Comput. Vis.*, 2014, pp. 127–141.

[38] D. Huang, L. Luo, M. Wen, Z. Chen, and C. Zhang, "Enable scale and aspect ratio adaptability in visual tracking with detection proposals," in *Proc. Brit. Mach. Vis. Conf.*, Sep. 2015, pp. 1–12.

[39] R. C. Gonzalez and R. E. Woods, *Digital Image Processing*. Upper Saddle River, NJ, USA: Prentice-Hall, 2007.

[40] X. Yu, F. Xu, S. Zhang, and L. Zhang, "Efficient patch-wise non-uniform deblurring for a single image," *IEEE Trans. Multimedia*, vol. 16, no. 6, pp. 1510–1524, Oct. 2014.

[41] H. K. Galoogahi, T. Sim, and S. Lucey, "Multi-channel correlation filters," in *Proc. IEEE Int Conf. Comput. Vis.*, Dec. 2013, pp. 3072–3079.

[42] P. Dollár. (Nov. 2014). *Piotr's Image and Video MATLAB Toolbox (PMT)*. [Online]. Available: http://vision.ucsd.edu/pdollar/toolbox/doc/index.html

[43] S. Zhang, S. Zhao, Y. Sui, and L. Zhang, "Single object tracking with fuzzy least squares support vector machine," *IEEE Trans. Image Process.*, vol. 24, no. 12, pp. 5723–5738, Dec. 2015.

[44] J. Zhang, S. Ma, and S. Sclaroff, "MEEM: Robust tracking via multiple experts using entropy minimization," in *Proc. Eur. Conf. Comput. Vis.*, 2014, pp. 188–203.

[45] M. Everingham, L. Gool, C. Williams, and A. Zisserman. (2005). *Pascal Visual Object Classes Challenge Results*. [Online]. Available: www.pascal-network.org

[46] Z. Kalal, K. Mikolajczyk, and J. Matas, "Tracking-learning-detection," *IEEE Trans. Pattern Anal. Mach. Intell.*, vol. 34, no. 7, pp. 1409–1422, Jul. 2012.

[47] X. Jia, H. Lu, and M.-H. Yang, "Visual tracking via adaptive structural local sparse appearance model," in *Proc. IEEE Conf. Comput. Vis. Pattern Recognit.*, 2012, pp. 1822–1829.

[48] T. B. Dinh, N. Vo, and G. Medioni, "Context tracker: Exploring supporters and distracters in unconstrained environments," in *Proc. IEEE Conf. Comput. Vis. Pattern Recognit.*, Jun. 2011, pp. 1177–1184.

[49] J. Kwon and K. M. Lee, "Visual tracking decomposition," in *Proc. IEEE Conf. Comput. Vis. Pattern Recognit.*, 2010, pp. 1269–1276.

[50] J. Kwon and K. M. Lee, "Tracking by sampling trackers," in *Proc. IEEE Int Conf. Comput. Vis.*, 2011, pp. 1195–1202.

[51] S. Yun, J. Choi, Y. Yoo, K. Yun, and J. Y. Choi, "Action-decision networks for visual tracking with deep reinforcement learning," in *Proc. IEEE Conf. Comput. Vis. Pattern Recognit.*, Jul. 2017, pp. 1349–1358.

[52] H. Nam and B. Han, "Learning multi-domain convolutional neural networks for visual tracking," in *Proc. IEEE Conf. Comput. Vis. Pattern Recognit.*, Jun. 2016, pp. 4293–4302.

[53] Y. Wu, J. Lim, and M.-H. Yang, "Object tracking benchmark," *IEEE Trans. Pattern Anal. Mach. Intell.*, vol. 37, no. 9, pp. 1834–1848, Sep. 2015.

[54] M. Kristan *et al.*, "A novel performance evaluation methodology for single-target trackers," *IEEE Trans. Pattern Anal. Mach. Intell.*, vol. 38, no. 11, pp. 2137–2155, Nov. 2016.

[55] S. Oron, A. Bar-Hillel, D. Levi, and S. Avidan, "Locally orderless tracking," *Int. J. Comput. Vis.*, vol. 111, no. 2, pp. 213–228, 2015.

[56] T. Zhang, B. Ghanem, S. Liu, and N. Ahuja, "Robust visual tracking via multi-task sparse learning," in *Proc. IEEE Conf. Comput. Vis. Pattern Recognit.*, 2012, pp. 2042–2049.

[57] P. Pérez, C. Hue, J. Vermaak, and M. Gangnet, "Color-based probabilistic tracking," in *Proc. Eur. Conf. Comput. Vis.*, 2002, pp. 661–675.

[58] B. Liu, J. Huang, C. Kulikowski, and L. Yang, "Robust visual tracking using local sparse appearance model and K-selection," *IEEE Trans. Pattern Anal. Mach. Intell.*, vol. 35, no. 12, pp. 2968–2981, Dec. 2013.

[59] D. Comaniciu, V. Ramesh, and P. Meer, "Kernel-based object tracking," *IEEE Trans. Pattern Anal. Mach. Intell.*, vol. 25, no. 5, pp. 564–577, May 2003.

[60] M. E. Maresca and A. Petrosino, "Clustering local motion estimates for robust and efficient object tracking," in *Proc. Eur. Conf. Comput. Vis.*, 2014, pp. 244–253.

[61] A. S. Montero, J. Lang, and R. Laganiere, "Scalable kernel correlation filter with sparse feature integration," in *Proc. ICCV Workshops*, 2015, pp. 587–594.

[62] G. Roffo and S. Melzi, "Online feature selection for visual tracking," in *Proc. Brit. Mach. Vis. Conf.*, 2016, pp. 1–12.

[63] M. Felsberg, "Enhanced distribution field tracking using channel representations," in *Proc. IEEE Int. Conf. Comput. Vis. Workshops*, 2013, pp. 121–128.

[64] J. Gao, H. Ling, W. Hu, and J. Xing, "Transfer learning based visual tracking with Gaussian processes regression," in *Proc. Eur. Conf. Comput. Vis.*, 2014, pp. 188–203.

[65] L. Sevilla-Lara and E. Learned-Miller, "Distribution fields for tracking," in *Proc. IEEE Conf. Comput. Vis. Pattern Recognit.*, Jun. 2012, pp. 1910–1917.

[66] K. Briechle and U. D. Hanebeck, "Template matching using fast normalized cross correlation," in *Proc. Aerosp. Defense Sens. Simul. Controls*, 2001, pp. 95–102.

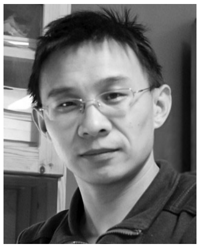

Shunli Zhang received the B.S. and M.S. degrees in electronics and information engineering from Shandong University, Jinan, China, in 2008 and 2011, respectively, and the Ph.D. degree in signal and information processing from Tsinghua University, Beijing, China, in 2016.

He is currently a Faculty Member with the School of Software Engineering, Beijing Jiaotong University, Beijing. His current research interests include pattern recognition, computer vision, and image processing.

Wei Lu received the B.S. degree in computer science from Fushun Petroleum Institute, Fushun, China, in 1985 and the M.S. degree in computer science and the Ph.D. degree in information and communication engineering from Sichuan University, Chengdu, China, in 1998 and 2006, respectively.

He is currently a Professor with the School of Software Engineering, Beijing Jiaotong University, Beijing, China. His current research interests include computer networks and information systems, and multimedia information processing.

Weiwei Xing received the B.S. and Ph.D. degrees in computer science from Beijing Jiaotong University, Beijing, China, in 2001 and 2006, respectively.

She is currently a Professor with the School of Software Engineering, Beijing Jiaotong University. Her current research interests include software engineering, computer vision, and image/video processing.

Li Zhang received the B.S., M.S., and Ph.D. degrees in signal and information processing from Tsinghua University, Beijing, China, in 1987, 1992, and 2008, respectively.

In 1992, he joined the Faculty of the Department of Electronic Engineering, Tsinghua University, where he is currently a Professor. His current research interests include image processing, computer vision, pattern recognition, and computer graphics.